Acoustic Liner Drag: Measurement Uncertainty Reduction and Application to Novel Perforate Geometries

Brian M. Howerton[1]
NASA Langley Research Center, Hampton, VA 23681-2199, USA

In addition to developing acoustic liner concepts and characterizing their performance, the NASA Langley Liner Physics Team has investigated issues related to liner drag. A method to quantify relative drag of liner configurations was developed and employed to understand the effects of various liner features. It was observed that perforate shape could have a marked effect on the measured liner drag and led to the discovery of a low-drag geometry that cut the drag penalty between a perforate and a smooth wall by approximately 50%. Investigations of novel perforates to further reduce drag were stymied by measurement uncertainty that prevented further resolution of drag differences between configurations. The current study details efforts to understand the causes of this uncertainty and describe changes made to testing methods to reduce it. Previously evaluated perforates were retested with these improvements in the NASA Langley Grazing Flow Impedance Tube to determine their relative drag at a flow speed of Mach 0.5 without acoustic excitation. Their performance was compared to the previously identified low-drag geometry to see if further drag reductions could be realized.

I. Nomenclature

a	=	duct width
b	=	duct height
c	=	speed of sound
d_h	=	duct hydraulic diameter
γ	=	ratio of specific heats
λ_{L+SW}	=	resistance factor of the liner plus the hardwall portion of the test section
λ_L	=	resistance factor of the liner
λ_{SW}	=	resistance factor of a smooth wall sample
LL	=	liner length
M	=	centerline flow Mach number
$p_{s\infty}$	=	static pressure, absolute
p	=	static pressure, differential
P_{atm}	=	atmospheric pressure
P	=	perimeter length of the test section
S	=	static pressure port separation distance
Q	=	duct dynamic pressure
W_L	=	width of liner
x	=	streamwise duct coordinate
ρ	=	density

[1] Research Scientist, Applied Acoustics Branch, MS 463, Senior Member AIAA, (brian.m.howerton@nasa.gov).

II. Introduction

In the quest to improve fuel efficiency of commercial aircraft for economic and environmental reasons, engine companies and airframers are continually looking for advances in design, materials and construction to drive down fuel burn. Achieving regulatory compliance for noise, however, can create issues as many of the technologies for reducing aircraft noise carry weight and/or drag penalties. Acoustic liners are one such technology and have been successful in reducing the radiated noise created by turbofan engines. Advances in the understanding of liner physics and design optimization coupled with new materials and manufacturing have made liners more effective and reduced the weight penalty associated with their use. When applying liners of the type shown in Fig. (1) to an engine or airframe configuration, it is assumed that some increase in drag would occur relative to those areas with smooth walls. This drag increase was accepted as a necessary tradeoff to use liners for noise reduction. The NASA Langley Liner Physics Team began investigating liner drag in 2013 with to quantify the drag penalty associated with liners and developing designs to minimize this penalty. Initial work saw the development of a technique to measure relative drag of liner configurations through calculation of the liner resistance factor (λ) developed by Nikuradse for flow in rough pipes [1-2]. Subsequently, parametric studies were performed to look at perforate hole size and cavity depth effects [2]. Results showed that for a given porosity, reducing hole size lowered values of λ (indicating lower drag) while doubling the cavity depth from 3.81 to 7.62 cm had no appreciable effect on the resistance factor. Howerton and Jones also investigated perforate geometries other than the conventional round holes and the effects of perforate orientation relative to the flow to improve liner drag performance [3].

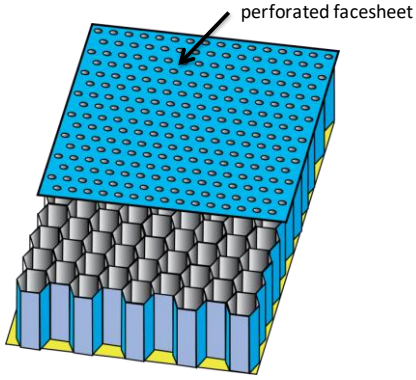

Fig. 1 Conventional liner construction

This work led to the discovery of a slot geometry, oriented with the long axis perpendicular to the flow, that significantly reduced the measured liner resistance factor. This new perpendicular slot geometry cut the difference in liner drag between a smooth wall and a conventional, round-hole perforate by approximately 50% without detrimental effect on the liner's acoustic performance (Fig. 2).

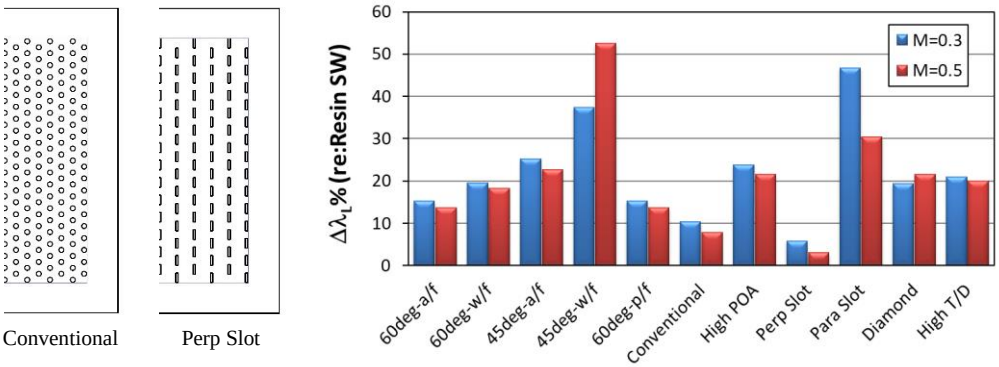

Fig. 2 Resistance factor increase relative to a smooth wall for various liner facesheet perforates.

Further experiments by the Liner Physics Team continued this work by evaluating a series of additively-manufactured perforates based on the Perpendicular Slot geometry [4]. It was hoped that these slot-derived configurations would offer further drag reduction relative to a similarly constructed resin, smooth-wall (RSW) baseline as shown in Fig. (3). Results were inconclusive, however, due to measurement uncertainty that rendered all the configurations statistically equal but still higher than the baseline.

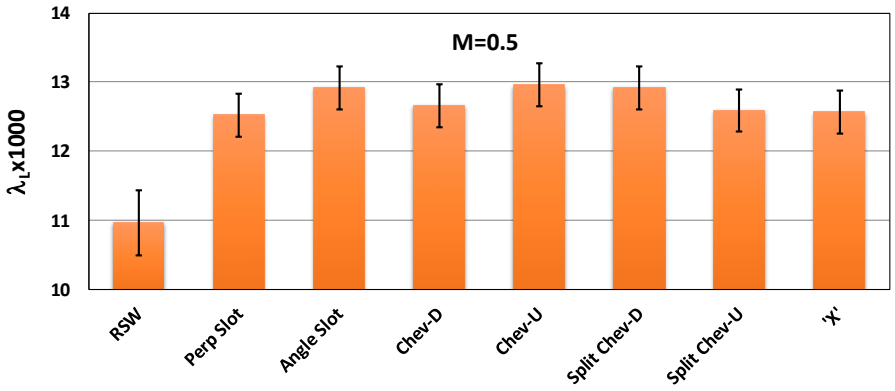

Fig 3 Comparison of slot-derived configurations with error estimates, Mach 0.5.

A study of drag measurement uncertainty using repeat runs of that RSW sample revealed significant variability over the course of two days of measurements. Comparisons of the drag data with available tunnel flow parameters produced apparent correlations with static temperature and pressure in the test section. It was postulated that some normalizing quantity could be determined that would reduce the measurement uncertainty such that these low-drag liner concepts could be reliably evaluated. This uncertainty reduction is needed to enable discovery of perforates that would meet NASA's goal of an 80% reduction in the liner drag penalty between conventional, round-hole perforates and a smooth wall.

The purpose of the current research effort is to understand the sources of uncertainty in the drag measurement process used at the NASA Langley Research Center Grazing Flow Impedance Tube (GFIT) and to evaluate reduction strategies through operational and measurement technique changes. Details are provided on the static pressure drop method used to compute λ along with a description of the liner samples tested. Once validated, drag measurements are made on these slot-derived perforates at Mach 0.5 and compared to results for the Perpendicular Slot design to find a perforate shape with even lower drag.

III. Liner Drag Measurements

A. Governing Equations

The method for determining relative liner drag relies on comparing differences in the static pressure drop measured along the duct wall opposite the liner samples. It is similar to Nikuradse's approach from his study of pipe roughness and can be applied to small ducts with fully-developed, turbulent flow [1]. From the static pressure data and selected flow parameters, one can compute the duct resistance factor, λ (also known as the 'friction factor'), given by the equation:

$$\lambda = \frac{dp}{dx}\frac{d_h}{Q} \tag{1}$$

where the hydraulic diameter of the flow duct (d_h) can be written as:

$$d_h = \frac{2ab}{a+b} \tag{2}$$

and the compressible form for Q is given by:

$$Q = \frac{\gamma}{2} p_{s\infty} M^2 \tag{3}$$

Note that λ encompasses the sum of the skin friction and pressure components of drag through the measurement of *dp*, which is modified by both. Thus, any effects of the liner cavity are also included, thereby differentiating this method from others that solely measure skin friction. The results of these calculations can be used to provide a relative measurement of drag between liner configurations.

From Ref. [3], the resistance factor for the lined portion of the duct (λ_L) can be given by:

$$\frac{\lambda_L}{\lambda_{SW}} = 1 + \frac{P}{W_L}\frac{S}{LL}\left(\frac{\lambda_{L+SW}}{\lambda_{SW}} - 1\right) \tag{4}$$

assuming that the contributions of any wall segment of the duct are proportional to segment surface area. The flush-mounted microphones are also assumed to have a negligible effect. Figure 4 provides a sketch of the GFIT test section showing typical liner placement and various pertinent dimensions required to evaluate this expression. Note that Eq. (4) requires a smooth-wall resistance factor (λ_{SW}) to compute λ_L. Tests using a machined aluminum block as the liner sample are used to calculate this value with results discussed in a later section.

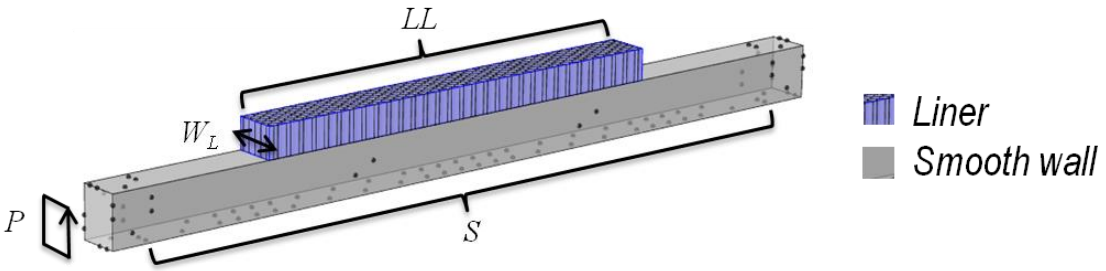

Fig. 4 Sketch of GFIT test section with dimensions used for liner drag eduction.

B. Resistance Factor Uncertainty

From Eq. (1), it is apparent that the variability in measured values of λ for a particular liner configuration comes from uncertainty in determining *dp* (static pressure drop along the liner) and *Q* (duct dynamic pressure) as *dx* (distance between static pressure ports measuring *dp*) and d_h (duct hydraulic diameter) are held constant. Static pressure drop is determined via direct measurement by a single pressure transducer. Thus, the uncertainty in any one measurement can be quantified from the transducer accuracy (assuming any bias is zeroed out and the instrument is calibrated correctly). Transducers of the type used here have accuracies based on a percentage of their full-scale measurement range. Therefore, for greatest accuracy, the transducer range must be comparable to the expected static pressure drop. Variability in dynamic pressure is less straightforward as it depends on tunnel static pressure, itself tied to P_{atm} and variable with time, and Mach number, which is tied to tunnel temperature.

The use of Eq. (4) to separate the resistance factor of the liner from the combination of liner and smooth wall is another source of uncertainty. Application of this expression requires two measurements of λ for both the metallic smooth wall and the combination of liner and duct smooth wall with the attendant uncertainty of each. Also, the ratio of lined and smooth wall areas between the static pressure ports used to measure *dp* has a direct effect on the uncertainty of λ_L. Reducing the separation distance between measurement ports, *S*, will increase this ratio which should lower resistance factor uncertainty.

Quantification of this variability in resistance factor was performed in Ref. [4] for the resin, smooth-wall plate (RSW) sample. Successive measurements of λ_L were made over two days to track how this quantity varied. Flow parameters from the GFIT were also logged to see if any correlations could be found between those parameters and the resistance factor results. The left plot of Fig. (5) shows the variation in λ_L over those two days for the RSW facesheet. The data show a trend toward increasing λ_L during each collection session. Repeatability within a given run or even for a collection session is good, but the shifts between sessions negatively affect the computed error estimate leading to a 95% confidence interval of +/- 4.23%.

The right plot of Fig. (5) is the GFIT static temperature (computed from the measured total pressure and isentropic relations) for each trial. Note that for a given run (five trials per run) the temperature generally increases. This increase resulted from efforts to maintain an adiabatic wall condition which was necessary at that time for impedance eduction methods. The flow in the GFIT heats the walls, and thus, raises their static temperature, which requires a further increase in the flow temperature to compensate. The overall trends with this parameter generally follow the behavior of the resistance factor plots in Fig. (5) suggesting a correlation. Similar behavior can be seen in other GFIT temperature data and implied that operating at a constant temperature may reduce the observed variability. The results

of this earlier study have led to the current GFIT procedure of having tunnel total temperature maintained at a constant 21 deg C (70 deg F).

Ideally, methods and instrumentation will be found to reduce the 95% confidence interval to something less than +/- 1%. This would allow for continued evaluation of low-drag perforates desired to meet the 80% drag penalty reduction goal stated earlier.

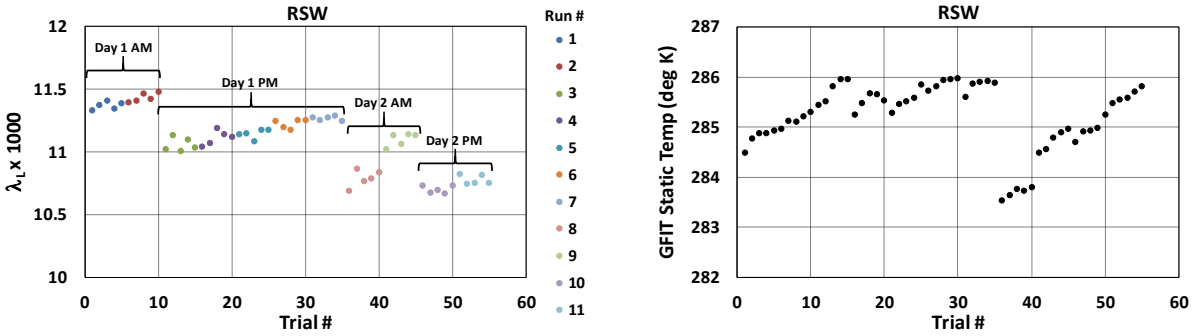

Fig. 5 Variation in resistance factor (λ_L) x 1000 with trial #, Mach 0.5, Ref. [4].

IV. Experiment

The experimental investigation involves two phases of testing with additively manufactured samples fabricated using a stereolithography process whereby liquid plastic resin is photopolymerized to build the part. For resistance factor measurement uncertainty testing, a resin smooth-wall sample (RSW) with no perforations is used to simulate a hardwall. Subsequent liner facesheet testing is done on five configurations with differing perforate geometries to determine resistance factors and characterize their acoustic performance. All perforate facesheets are constructed to have a percent open area (POA) of eight. For each sample, a high-accuracy measurement of the axial static pressure drop across the liner is made to compute the resistance factor. Customarily, this measurement is performed with and without acoustic excitation, but only no-sound results are presented here.

A. Resistance Factor Uncertainty

The process of measuring the quantities used in computing λ_L for a given liner sample involves several physical/procedural steps that could introduce uncertainty. Additionally, variation could occur if the proper test conditions are not held constant as noted earlier. To quantify the influence of these factors on measurement uncertainty, a series of experiments are performed to determine λ_L over a series of 11 measurement runs with 5 measurements (trials) in each. Table 1 summarizes the experiments.

Table 1. Uncertainty testing nomenclature.

Test Nomenclature	Measurement Conditions
Order 0	55 successive repeat trials, constant flow conditions (constant T_t)
Order 1	11 measurement runs (5 trials each), flow restarted for each run
Order 2	11 runs, flow restarted and sample reinstalled for each run
Order 3	11 runs over 11 days, flow restarted, sample reinstalled for each (Constant Mach)

The Order 0 tests involve installing the RSW sample, achieving the desired flow conditions then taking successive measurement sets. It is thought that operating at a constant total temperature will reduce the variability observed in Fig. 5 for this same configuration. These tests should also set a floor for uncertainty as the number of varying parameters is minimized and there are no physical/procedural steps between runs.

For Order 1 testing, the sample is left in place, but the flow is stopped and restarted between each run. This should give some indication on how well the GFIT flow conditions can be repeated. Order 2 incorporates the additional step of removing and replacing the sample in the test section. Inconsistencies related to steps and gaps potentially created by the installation process should become apparent from this phase of testing. Bringing in the effects of environmental variability is the aim of Order 3 testing, as each measurement run is performed on a different day. Since the static

pressure in the test section is matched to atmospheric pressure, changes in P_{atm} will result in different settings for the tunnel run condition. For this study, the GFIT is operated using constant flow Mach number as the setpoint.

B. Liner Facesheet Construction

For this investigation, several perforate geometries utilizing various slot geometries that build upon the results from Howerton and Jones [3] are investigated. A facesheet using the perpendicular slot previously constructed for that study is included for comparison. Details of the perforate shapes and dimensions are provided in Fig. (6). The angled configurations are intended to induce a spanwise velocity to the flow while the two chevron perforates are an attempt to create longitudinal vorticity similar to the riblet low-drag treatments studied by various entities [5-7]. Note that the chevron-based configurations are tested in the orientation as shown in Fig. (6) noted by a '-D' in later figures) and again in a reversed orientation ('-U') to determine the effects of relative flow direction.

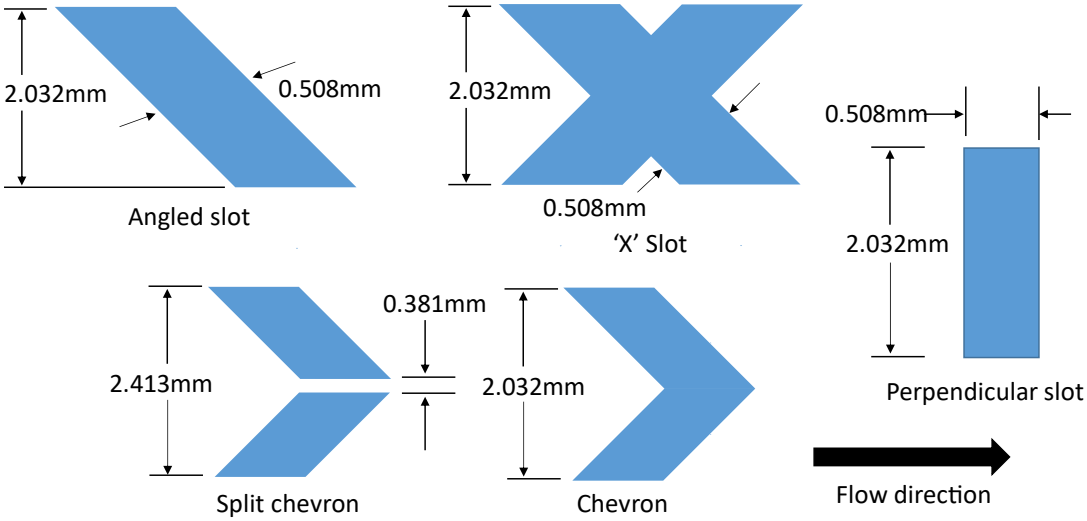

Fig. 6 Facesheet perforate geometry (not to scale).

C. Liner Core Construction

Each facesheet was mounted onto a metallic liner core with a cavity depth of 38.1 mm. To allow for rapid changes of liner configuration, the facesheets are not bonded to the core structure but taped to the liner box and clamped by their long edges as part of installation in the test rig. Note that the core is constructed for the full length of the GFIT test window (614.4 mm, 24 in.) while the facesheets are only 460.8 mm (18 in.) long due to printer limitations. The liner core is aluminum and comprised of regularly arranged hexagonal cells with a flat-to-flat cell dimension of 9.525 mm (0.375 in.). An aluminum filler blank of the same thickness was fabricated to cover the remaining portion of the core. Figure 7 shows a typical arrangement with the filler blank (right) and the facesheet (left) overlaid on the core. Note that when the sample is installed in the GFIT, flow would travel from left to right.

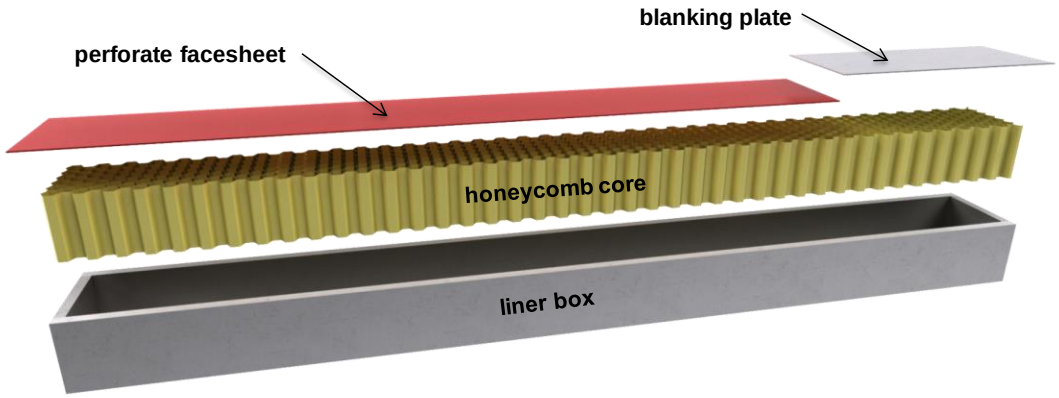

Fig. 7 Typical liner sample.

D. Grazing Flow Impedance Tube (GFIT)

The NASA Langley GFIT facility is routinely used to determine the acoustic characteristics of noise reduction treatments (acoustic liners) for aircraft jet engine nacelles and nozzles. With the addition of some high-accuracy pressure instrumentation, however, calculations can be made of liner friction factors to evaluate drag performance. The facility is a wind tunnel with a 50.8 mm by 63.5 mm (2 in. by 2.5 in.) rectangular cross section. The flow path (Fig. 8) consists of a straight duct with an upstream acoustic source section using 12 drivers, interchangeable lengths of blank duct, a test section where the liner sample is held along the upper wall of the duct and an array of 95 measurement microphones leading to a 12-driver downstream source section. Near-anechoic terminating diffusers are employed at each end of the duct to control reflections and reduce overall flow noise. The source sections can generate sound pressure levels up to 150 dB for the frequency range between 400 and 3000 Hz. Pressurized, heated air is supplied to the entrance of the GFIT in conjunction with a vacuum system at the duct exit to provide the flow in the tube. The static pressure at the test section can thus be held near ambient at all flow velocities. Temperatures are measured by Type-K thermocouples located in the tunnel pitot-static probe and embedded in the test section wall. Grazing flow velocities from Mach 0.0 to Mach 0.6 are available with such an arrangement.

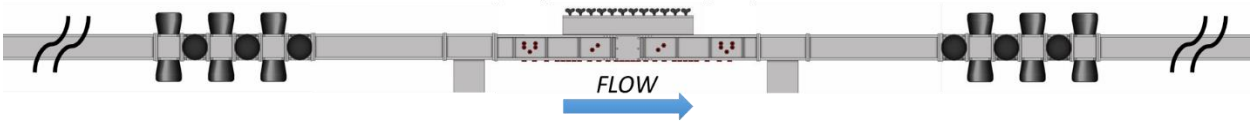

Fig. 8 Sketch of the NASA Langley Grazing Flow Impedance Tube (GFIT).

The lower wall of the GFIT contains 80 static pressure ports to measure the axial pressure distribution. A pair of those ports (separated axially by 1.07 m) bracket the test section liner opening and are used in the pressure drop measurement (henceforth referred to as the *wide* arrangement). They are connected to a high-accuracy, differential pressure gauge (pressure transducer) to measure the static pressure drop between these two locations. The gauge has a 0-6900 Pa range and 0.01% full-scale accuracy sampling at a rate of ~2 Hz. A plot of the static pressure distribution in the test section for a smooth wall configuration at Mach 0.5 is given in Fig. (9). The relative location of the liner and the ports used to compute the static pressure drop are given in a sketch of the test section included above the plot. The measurement points for this wide arrangement are designated as Ps_1 and Ps_2.

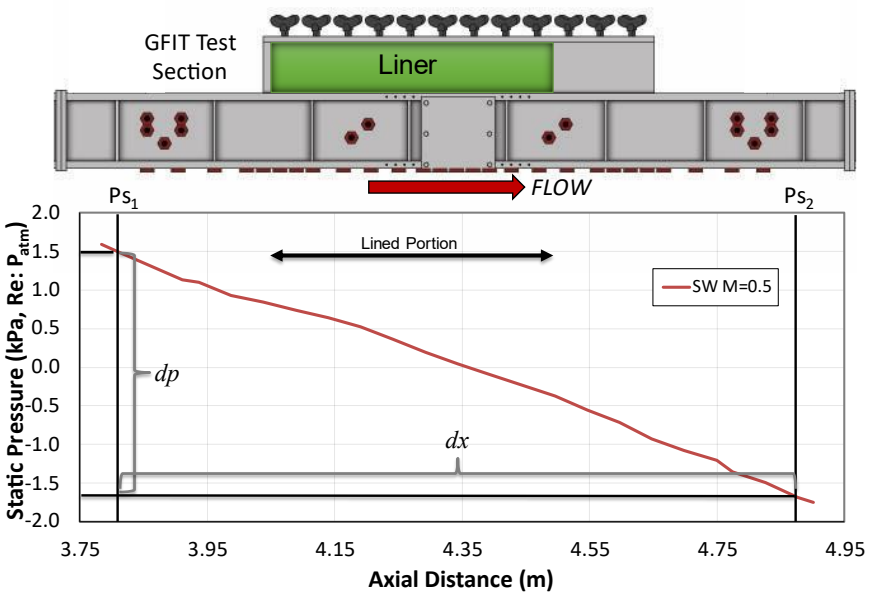

Fig. 9 GFIT Test Section Static Pressure Distribution, Smooth-wall sample, Mach 0.5.

Modifications are made to this arrangement to reduce measurement uncertainty. An additional set of static pressure ports are used where the spacing between the ports, Ps_3 and Ps_4, was reduced from 1.07 m to 0.81 m (referred to as the *narrow* arrangement). The change increased the ratio of lined-to-unlined area within the duct measurement volume.

This corresponds to a reduction of S in Eq. (4) which should decrease uncertainty in λ_L by a similar percentage. With the current values for S and LL, the liner resistance factor is very sensitive to small changes in dp, but this sensitivity should be reduced for a smaller S. Theoretically, the calculated resistance factor values should be independent of port spacing, but this test should verify that assumption. In conjunction, a second measurement array of pressure transducer instruments is used where the calibrated pressure range is tailored to the expected dp at Mach 0.3, 0.5 and 0.6 (PT1, PT2 and PT3 in Fig. (10)). This corresponds to maximum ranges of 2500, 4275 and 6900 Pa (0.36, 0.60 and 1.0 psi), respectively, with the same 0.01% accuracy (as noted previously) reducing the uncertainty in dp by 40 to 65%. Overpressure protection of the lower-range transducers is accomplished via computer-controlled solenoid valves to route Ps_3 to the proper transducer based on GFIT flow Mach number. Ps_4 provides the reference pressure for all measurements regardless of Mach number, as shown in Fig. 10.

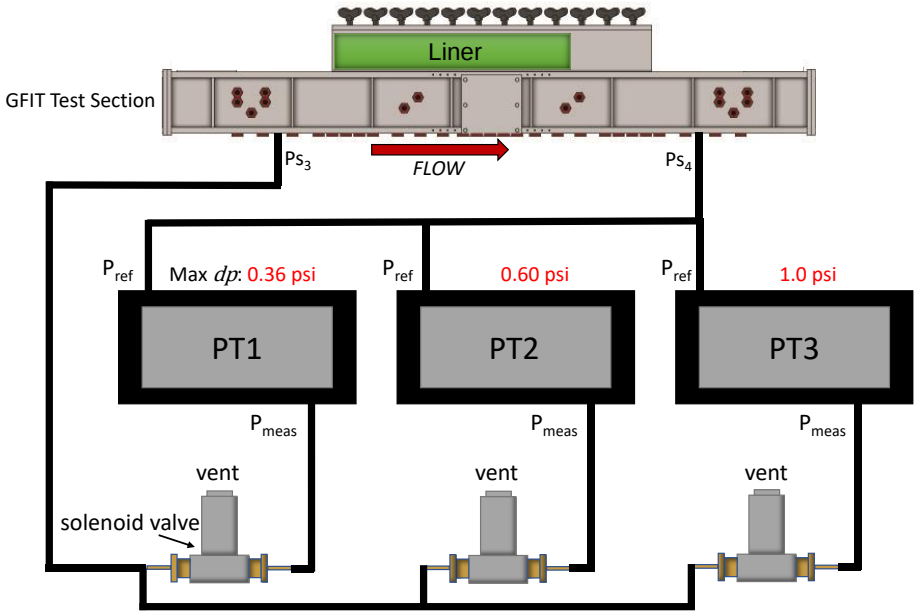

Fig. 10 Configuration of static pressure measurement for the narrow arrangement.

E. Measurement Process

The measurement process follows the method used by Howerton and Jones [3] where averaged static pressure measurements are made for each configuration with no acoustic excitation at Mach 0.5. For each data set, 300 readings are acquired from each pressure gauge to provide the static pressure drop between both sets of static pressure measurement ports (wide and narrow). Tunnel conditions, including average Mach number and static pressure, are also recorded to compute λ_L from Eq. (4). Uncertainty was determined by calculating the 95% confidence interval using +/- two standard deviations from the mean value of λ_L from the 55 trials.

V. Results and Discussion

A. Liner Drag Uncertainty

1. Smooth-wall Sample Results

As stated earlier, a measurement of the resistance factor for a smooth-wall sample, λ_{SW}, is required for subsequent determination of λ_L for a given liner sample. This is accomplished through testing of a machined, aluminum block as the sample. Figure 11 is a plot of that measured value for 11 runs at Mach 0.5 with no sound for the wide port arrangement. The data was acquired over the course of 11 days (1 run per day) to include any effects of atmospheric variance. The left plot shows values of λ_{SW} computed using Eq. (1) while the right plot are the results for λ_{SWL} from applying Eq. (4) with the λ_{SW} value. In theory, both calculations should produce the same answer and do so in the aggregate. There are, however, significant differences in individual values and the resultant uncertainties. Repeatability of the λ_{SW} measurement is quite good with an overall uncertainty of +/- 0.58% with values tightly

clustered between 10.2 and 10.4x10^{-3}. Using Eq. (4) increases uncertainty by an order of magnitude to +/- 6.1% as evidenced by the much wider spread in λ_{SWL} values.

Similar results are shown in Fig. 12 when using data from the narrow port spacing. There is an obvious difference in the average resistance factor with a lower value calculated for the narrow port arrangement as seen in Table 2. Since the data for both calculations were acquired simultaneously and the equations factor in port spacing, the values should match. The discrepancy indicates the existence of some feature within the duct, between the narrow and wide port locations, that increases the static pressure drop. Likely candidates are the clusters of flush-mounted microphones circumferentially placed between Ps_1 and Ps_3 as well as between Ps_4 and Ps_2. Their presence could be a source of additional roughness that increased the resistance factor values for the wide port calculations. Uncertainty values are

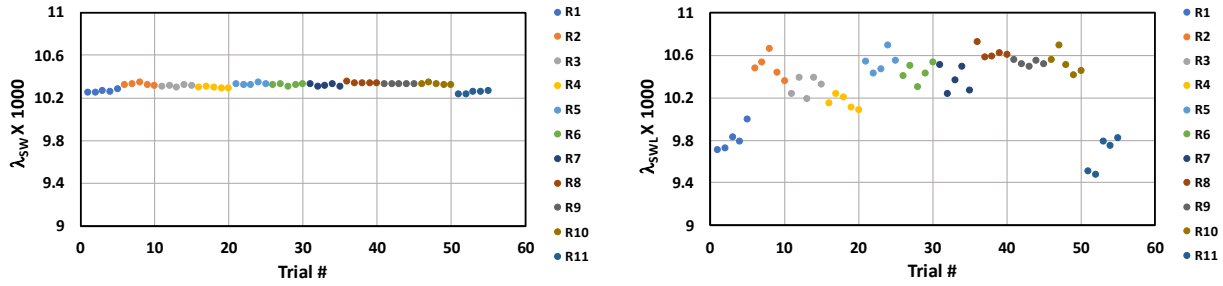

a) From Eq. (1) **b) From Eq. (4)**

Fig. 11 Computed smooth-wall resistance factor, M=0.5, no sound, *wide* port arrangement.

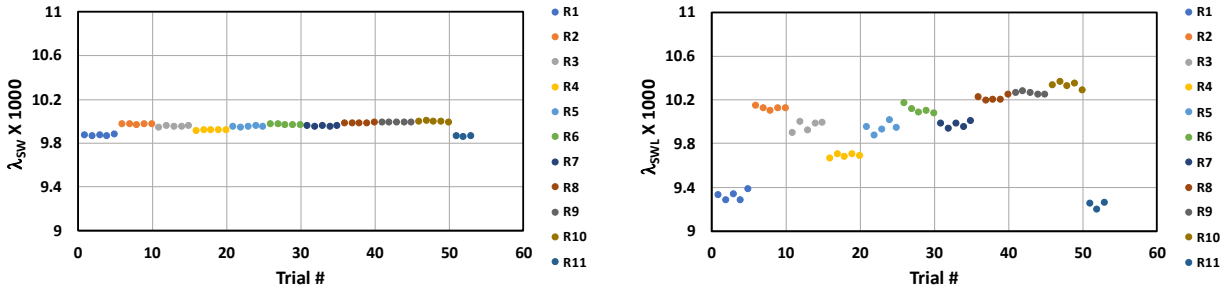

a) From Eq. (1) **b) From Eq. (4)**

Fig. 12 Computed smooth-wall resistance factor, M=0.5, no sound, *narrow* port arrangement.

slightly higher for the narrow port results (Table 2) which is opposite the expectation for this arrangement when using Eq. (4).

When evaluating these resistance factors and uncertainties, it is critical to understand the scale and precision required in measuring the physical quantities needed for their calculation. As an example, the maximum and minimum values in Fig. (11b) differ by ~1.25 but the change in *dp/Q* required to create that delta is only 0.0022.

Table 2. Computed resistance factors and uncertainty for the smooth-wall sample, M=0.5, no sound.

Computed values	Wide	Narrow
λ_{SW} x 1000	10.3122	9.947554
% uncertainty: Eq. (1)	0.58	0.82
% uncertainty: Eq. (4)	6.11	6.6

2. Resin Smooth-Wall Sample Results

Data from the RSW sample for the Order 0 case with the GFIT operating at Mach 0.5 and at a constant total temperature are shown in Fig. (13). It is important to remember that this set of measurements is acquired by setting the GFIT flow conditions, waiting for them to stabilize, then taking all 55 trials in succession. As such, the results should produce the lower limit of uncertainty for the measurement method with this instrumentation and procedures. The first thing to note is the overall difference in resistance factors computed for the wide and narrow port arrangements. The wide port values are in keeping with those recorded in earlier studies using this sample but are

approximately 5% higher than measured in Ref. [4]. The wide spacing produces slightly higher values for λ_L in each case where the expectation was for the values to be very similar. The explanation postulated earlier concerning the microphone locations for the smooth-wall sample would apply here as well. It is also quite apparent that the narrow port spacing results in significantly less variability in the computed values of λ_L as compared to the wide spacing (uncertainty values of 0.83% vs. 1.89% respectively). While some improvement was expected for reasons discussed earlier, the calculated uncertainty was cut by approximately 55% (see Table 3). This effect was greater than anticipated from the improved accuracy of the narrow port spacing's pressure transducer and more favorable ratio of lined-to-unlined duct wetted area in the λ_L calculation.

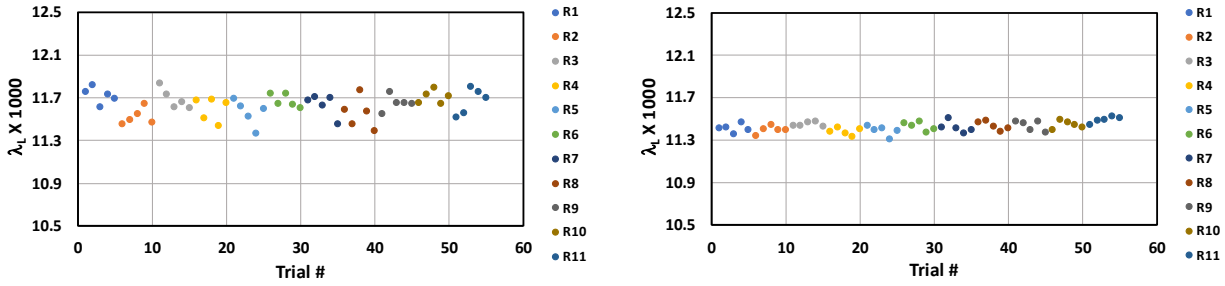

a) Wide **b) Narrow**

Fig. 13 Computed RSW resistance factor, Order 0, M=0.5, no sound.

The effect of starting and stopping the flow between runs on λ_L (Order 1) can be seen in Fig. (14). This test should assess how well tunnel flow conditions can be set for the GFIT given the adjustments offered by the rig's process control system. Average values for liner resistance factor are nearly identical to those for Order 0. However, the calculated uncertainty percentages nearly doubled to 3.28% for the wide port configuration and 1.38% for the narrow port arrangement (Table 3). Operating tolerances for GFIT are to keep Mach number to within +/- 0.002 of desired and can usually be set to within 0.001. Tunnel total temperature is set to within +/- 0.28 degC (0.5 degF) and test section static pressure is targeted to be within +/- 69 Pa (0.01 psi) of P_{atm}. It is not likely that these tolerances could be tightened further without significant effort and modifications to the control system. Some consideration was also given to whether any of the resistance factor values could be statistical outlier points that should be rejected from the uncertainty calculations. Trial 15 from the wide port dataset and trial 54 from the narrow set seemed possible candidates. Both PaHTa's rule and Thompson's tau test for determining statistical outliers were applied to the datasets but no points meeting their rejection criteria were found.

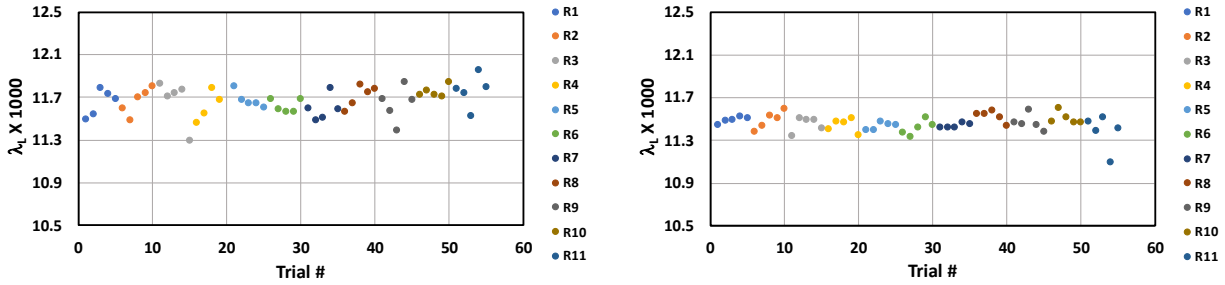

a) Wide **b) Narrow**

Fig. 14 Computed RSW resistance factor, Order 1, M=0.5, no sound.

Order 2 testing added the step of physically removing and reinstalling the RSW sample in the GFIT to determine if there were any inconsistencies in mounting the sample. The design of the test window limits sample insertion depth to guarantee flushness with the rest of the duct. As the sample must be slightly shorter than the test window opening (~0.127 mm to allow for insertion), there is a potential for small gaps at the sample leading and trailing edges which could influence the measurement. Note that due to the time required for each run, it took two days to complete the testing. Figure 15 plots the resistance factor results for Order 2 using both the wide and narrow port spacings. Average values were just slightly higher as compared to Orders 0 and 1. Surprisingly, uncertainty for the wide port measurements decreased relative to Order 1 while a small increase was seen in the narrow port spacing results. As testing for Orders 0-2 were performed on successive days, it is possible that operator skill in achieving and maintaining

the desired test conditions improved over time which would reduce uncertainty. Further work will be required to evaluate this hypothesis. The results, however, suggest that sample mounting is not a key contributor to resistance factor measurement uncertainty. The observed uncertainty reduction between the wide and narrow port spacings was approximately 30% and in keeping with expectations.

Calculations of λ_L for these three orders all used the average smooth-wall sample values from Table 2 for λ_{SW} in Eq. (4). For each day of Order 2 testing, the smooth-wall sample was also measured such that a λ_{SW} value could be

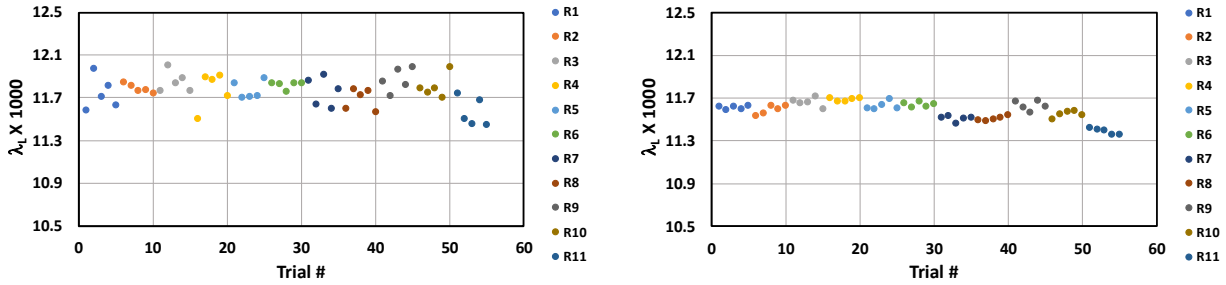

a) Wide **b) Narrow**

Fig. 15 Computed RSW resistance factor, Order 2, M=0.5, no sound.

calculated for use in processing that day's RSW sample data. Having a daily value for smooth-wall resistance factor should help to normalize variations in multi-day testing. This theory was not supported by the data as average values for resistance factors and uncertainty for both processing methods and port spacings produced almost identical results and are not shown for the sake of brevity. As the computed daily values for λ_{SW} were very close to the average, the outcome was not unexpected.

For Order 3, the RSW sample was tested over 11 days with measurements for one run of five trials performed each day. Like Order 2, the sample was removed and re-installed each day. The purpose this procedure was to determine the influence of day-to-day variation in properties like test section static pressure (which varies with P_{atm}) or wall static temperature (influenced by room temperature). Results for this testing are given in Fig. (16) for both static port spacings. Average values for λ_L are consistent with earlier testing but the computed uncertainty increases to 6.38 and

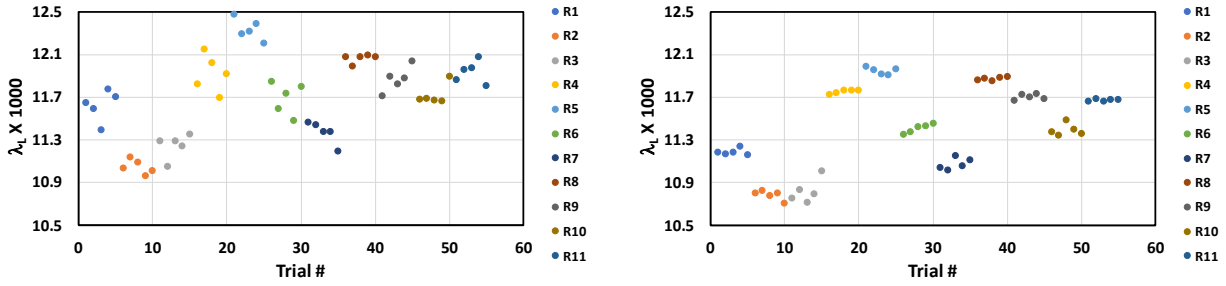

a) Wide **b) Narrow**

Fig. 16 Computed RSW resistance factor, Order 3, M=0.5, no sound.

6.77% for the wide and narrow port configurations respectively. Whereas previous testing showed the benefits of reducing the static port spacing on uncertainty, that benefit is not seen here. It is apparent that some physical property or combination properties not held consistent each day, is responsible for producing this variation. The effect also overwhelms the benefits previously observed for the narrow port configuration. No variations of the GFIT flow parameters and physical quantities measured or calculated (including various pressures, temperatures, Mach and Reynolds numbers), seem to correlate with the observed daily RSW resistance factor variation.

Table 3. Computed uncertainty results (%).

Test Nomenclature	Wide	Narrow
Order 0	1.89	0.83
Order 1	3.28	1.38
Order 2	2.21	1.51
Order 3	6.38	6.77

B. Drag Comparison

After RSW sample testing for selected days of the Order 3 investigation, the slot-derived liner facesheet samples were also evaluated for drag in the GFIT. Testing was accomplished over five days where one run of five trials was performed for each liner with the average λ_L results shown in Fig. (17) and (18). Included are values for the smooth-wall (SW) and the RSW samples for comparison. Error bars are applied using the uncertainty values for each port spacing from Table 2, Eq. (4) for the HW sample and the Order 3 results in Table 3 for the RSW and slot-derived facesheet samples.

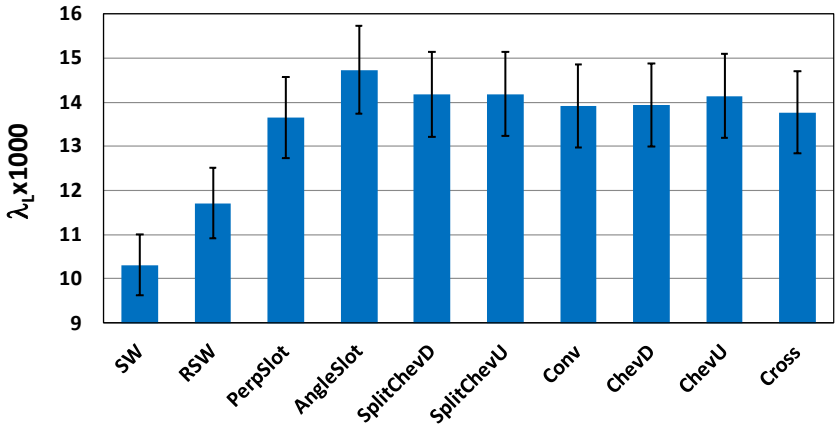

Fig. 17 Comparison of λ_L for selected configurations with error estimates, Mach 0.5, no sound, wide port configuration.

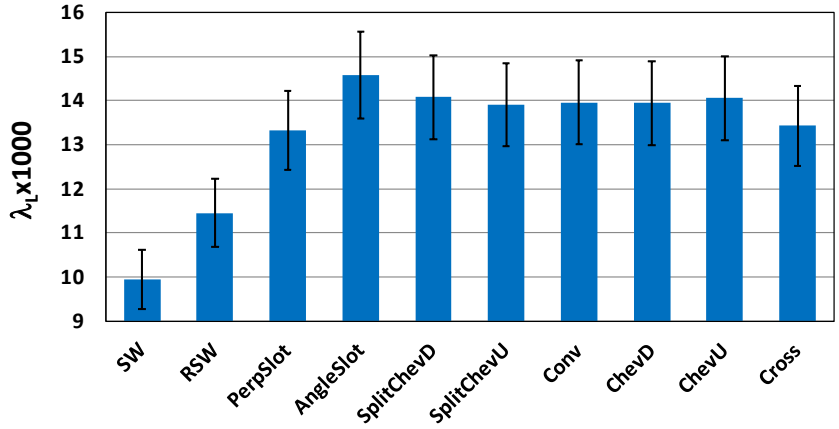

Fig. 18 Comparison of λ_L for selected configurations with error estimates, Mach 0.5, no sound, narrow port configuration.

The lowest values for λ_L are produced by the smooth-wall sample (SW), as one would expect, followed by the resin smooth-wall (RSW) regardless of measurement port spacing. For the remaining configurations, the uncertainty is such that no statistically significant difference exists between any of them. Therefore, one cannot determine accurately if any of these configurations performs better than the Perpendicular Slot design previously identified as providing a drag reduction benefit [3]. The results from the uncertainty study suggest that comparative liner drag

measurements of a set of samples should likely be performed in a single day and include a smooth-wall sample measurement to minimize uncertainty.

VI. Conclusion

A series of experiments were performed to determine the uncertainty associated with the liner drag measurement process currently employed in the NASA Langley Grazing Flow Impedance Tube. A machined aluminum sample provided the smooth-wall value while an additively-manufactured resin smooth-wall sample was used as a baseline reference for determining the resistance factor, λ_L, for the various samples tested. The effects of instrumentation and test method changes were evaluated along with efforts to understand the effects of certain procedural aspects on measurement uncertainty. Some observations are as follows:

1. Back-to-back repeatability for the drag measurement process (Order 0) is very good with measured uncertainty values of less than 1%.

2. Reducing the distance between measurement ports, in conjunction with instrumentation better matched to the expected static pressure drop values, generally provided reduced measurement uncertainty for all orders tested except Order 3 where this benefit appears to disappear.

3. Even with the tight Mach number, static pressure and total temperature tolerances used when setting up a flow condition in the GFIT (Order 1), the effect of these variations results in a near doubling of the uncertainty in λ_L relative to Order 0. It is unlikely that further reductions in these tolerances can be easily achieved.

4. The process of mounting the sample in the GFIT appears to be consistent such that removing and reinstalling the sample produces little effect on the resistance factor calculated uncertainty (Order 2).

5. Uncertainty values calculated from repeat testing over multiple days were significantly larger than seen from any of the other orders (Order 3). It is unclear what parameters are not being held constant to reduce or eliminate this day-to-day variability. The effect is large enough to overwhelm the benefits observed in lower order testing from instrumentation and port spacing changes.

6. With the current method, the differences between liner samples tested for drag over multiple days may not be statistically meaningful as seen when evaluating a set of slot-derived liner facesheets. It may be necessary for such testing to occur in a single day in order to make relevant comparisons until further improvements to the method can be made.

Future work should focus on determining the cause of increased variability when testing over multiple days. This will be critical when studying the combined effects of acoustic and drag as such testing takes significantly more time than drag measurements alone. Improvements to the method will also be necessary to determine if there exists other facesheet perforates with better drag characteristics than the Perpendicular Slot design developed nearly a decade ago.

Acknowledgments

The authors would like to thank Martha Brown and Alonzo ‘Max’ Reid from the NASA Langley Aeroacoustics Branch for their efforts in collecting the experimental data. This research was conducted in support of the NASA Advanced Air Transport Technology Project for the Advanced Air Vehicles Program.

References

[1] Nikuradse, J., “Laws of Flow in Rough Pipes,” NACA TM-1292, November 1950.
[2] Howerton, B. M., and Jones, M. G., “Acoustic Liner Drag: A Parametric Study of Conventional Configurations,” AIAA Paper 2015-2230, June 2015.
[3] Howerton, B. M., and Jones, M. G., “Acoustic Liner Drag: Measurements on Novel Facesheet Perforate Geometries,” AIAA Paper 2016-2979, June 2016.
[4] Howerton, B. M., and Jones, M. G., “Acoustic Liner Drag: Further Measurements on Novel Facesheet Perforate Geometries,” AIAA Paper 2018-3605, June 2018.
[5] Viswanath, P. R., “Aircraft viscous drag reduction using riblets,” *Progress in Aerospace Sciences*, Vol 38, No. 6-7, 2002, pp. 571-600.

[6] García-Mayoral, R., and Jiménez, J., "Drag reduction by riblets," *Philosophical transactions of the Royal society A: Mathematical, physical and engineering Sciences*, Vol. 369, No. 1940, 2011, pp. 1412-1427.
[7] Walsh, M. and Lindemann, A., "Optimization and application of riblets for turbulent drag reduction," AIAA Paper 1984-347, Jan 1984.